Geophysical Research Letters

RESEARCH LETTER
10.1029/2021GL093785

Key Points:

- Based on geodetic data, the San microplate in southern Africa is distinct from the Nubian Plate with a boundary that follows active rifts
- New Global Navigation Satellite System data show the southern Malawi Rift has an extension rate of 2.2 ± 0.3 mm/yr with 75% of relative velocity in a region 890 km wide
- In thick continental lithosphere, strain accumulates over broad zones but seismicity concentrates in narrower zones at the edge of cratons

Supporting Information:

Supporting Information may be found in the online version of this article.

Correspondence to:

L. N. J. Wedmore,
luke.wedmore@bristol.ac.uk

Citation:

Wedmore, L. N. J., Biggs, J., Floyd, M., Fagereng, Å., Mdala, H., Chindandali, P., et al. (2021). Geodetic constraints on cratonic microplates and broad strain during rifting of thick southern African lithosphere. *Geophysical Research Letters*, *48*, e2021GL093785. https://doi.org/10.1029/2021GL093785

Received 24 MAY 2021
Accepted 8 JUN 2021

Geodetic Constraints on Cratonic Microplates and Broad Strain During Rifting of Thick Southern African Lithosphere

L. N. J. Wedmore[1], J. Biggs[1], M. Floyd[2], Å. Fagereng[3], H. Mdala[4], P. Chindandali[5], J. N. Williams[3], and F. Mphepo[4]

[1]School of Earth Sciences, University of Bristol, Bristol, UK, [2]Department of Earth, Atmospheric and Planetary Sciences, Massachusetts Institute of Technology, Cambridge, MA, USA, [3]School of Earth and Environmental Sciences, Cardiff University, Cardiff, UK, [4]Geological Survey Department, Mzuzu Regional Office, Mzuzu, Malawi, [5]Geological Survey Department, Zomba, Malawi

Abstract Southern Africa is typically considered to belong to a single tectonic plate, Nubia, despite active faulting along the southwestern branch of the East African Rift System. We analyze regional Global Navigation Satellite System (GNSS) measurements, and find that the "San" microplate, situated south of the southwestern branch of the East African Rift, is statistically distinct from Nubia, with 0.4–0.7 mm/yr of extension across the boundary. Adding nine new campaign GNSS sites, we show that the extension rate across the southern Malawi Rift is 2.2 ± 0.3 mm/yr, with 75% of the relative velocity occurring over 890 km, despite the surface expression of faulting being <150 km wide. Thus, for the first time, we use geodetic measurements to describe the accommodation of strain in broad zones between Archean cratons in southern Africa's thick continental lithosphere.

Plain Language Summary The breakup of continental plates is a fundamental part of plate tectonics, but little is known about how the plates start to stretch. In southern Africa, which is slowly extending, we use Global Positioning System (GPS) instruments to precisely measure the motion of the plates. Statistical tests show that southern Africa, which had previously been modeled as a single rigid plate called Nubia, can be better modeled as two separate plates, by the addition of the San microplate in southern Africa. We find that the plate-boundary in southern Malawi is extending at ∼2 mm per year. However, the region that is actively extending is 890 km wide, which is wider than the 150 km wide region where we observe earthquakes and faults. Our new geodetic constraints suggest that in southern Africa, the continental plates are stretching apart at weaknesses around multiple microplates of old, thick crust, rather than along one single plate boundary.

1. Introduction

Understanding strain distribution and kinematics during early stage continental rifting remains a fundamental challenge in plate tectonics. For example, the stresses responsible for amagmatic continental extension of the East African Rift System (EARS) are enigmatic (Kendall & Lithgow-Bertelloni, 2016), despite this being the best exposed active continental rift system on the Earth's surface (Corti, 2009; Ebinger, 2005). The enigma arises because plate boundary forces, dynamic topography, horizontal tractions, and gravitational potential energy do not provide sufficient stress to break the thick, cold continental lithosphere of cratonic Africa (Kendall & Lithgow-Bertelloni, 2016). Earthquakes are predominately confined to Proterozoic orogenic belts at the edges of Archean cratons (Figure 1a; e.g., Daly et al., 1989; Manzunzu et al., 2019; Midzi et al., 2018; Yang & Chen, 2008), but because global seismic networks are only able to detect events with $M > \sim 4.5$, detailed kinematic information from seismicity is only available from limited local and regional studies (e.g., Craig & Jackson, 2021; Ebinger et al., 2019; Lavayssière et al., 2019).

Global Navigation Satellite System (GNSS) observations can provide a better spatial understanding of plate kinematics, but because stations are sparsely distributed in southern Africa, many possible plate boundary configurations have been proposed (Calais et al., 2006; Daly et al., 2020; Fernandes et al., 2004; Saria et al., 2013, 2014; Stamps et al., 2008, 2020). In initial studies, Africa was divided along a single, linear rift system into the Somalian and Nubian plates (Fernandes et al., 2004; Jestin et al., 1994). Subsequent studies

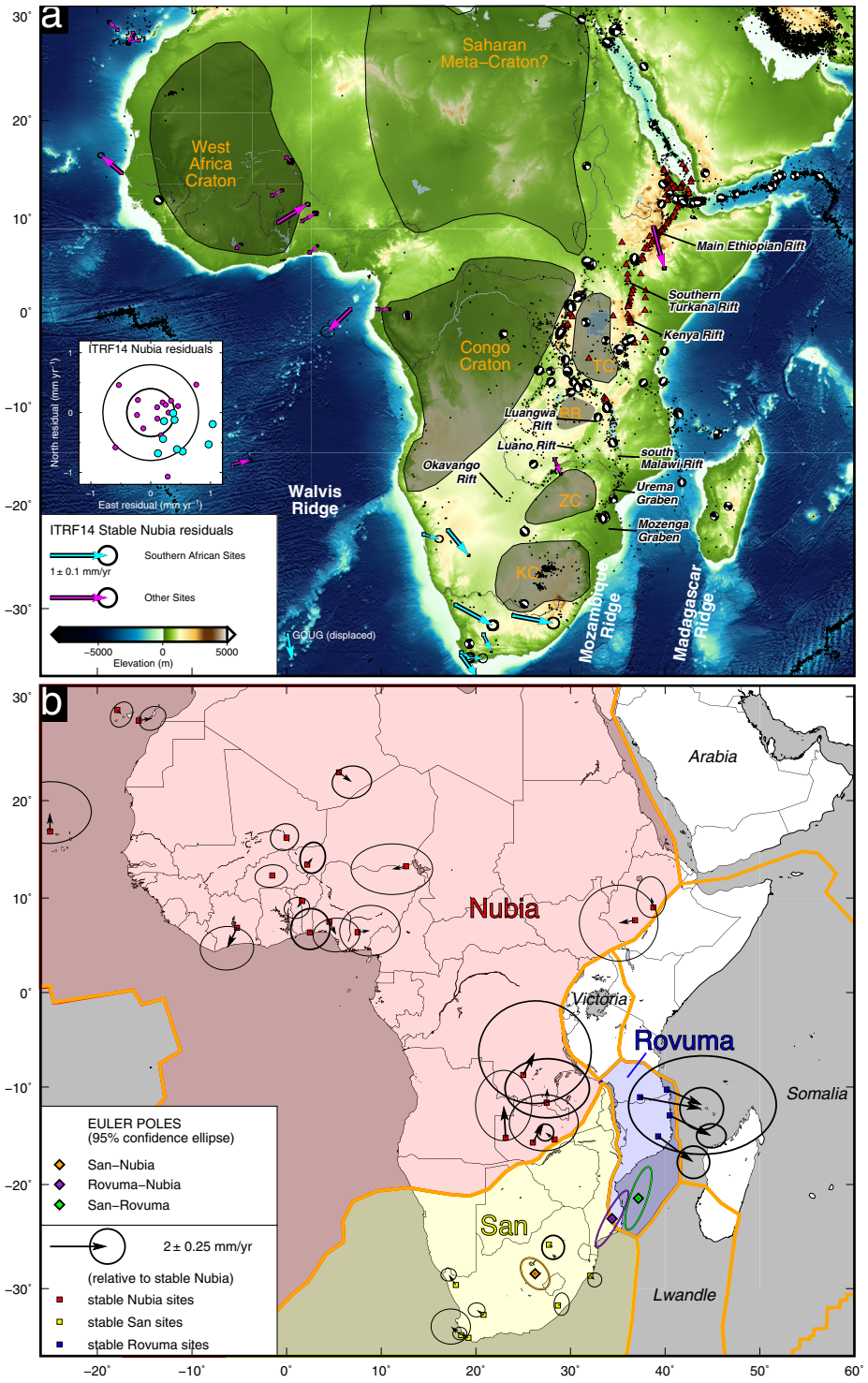

Figure 1. Seismotectonics and plate configuration of Africa. (a) The Global Positioning System stations used to define stable Nubia in the ITRF2014 plate motion model and their residuals plotted alongside the distribution of earthquakes ($M_w > 3$), earthquake focal mechanisms ($M_w > 5.5$; Craig et al., 2011), topography (Becker et al., 2009), Holocene active volcanoes (red triangles), and Archean and Paleoproterozoic craton boundaries (adapted from Van Hinsbergen et al., 2011). Inset is a plot of the ITRF2014 residual velocities, with the sites in southern Africa plotted in yellow. BB, Bangweulu Block; KC, Kaapvaal Craton; TC, Tanzania Craton; ZC, Zimbabwe Craton. (b) Our plate angular velocity solution showing the movement of sites used to define the San (yellow shading) and Rovuma (blue shading) relative to stable Nubia (red shading), and the Euler poles from our velocity solution. Orange lines are plate boundaries (adapted from Daly et al., 2020; Saria et al., 2013; Stamps et al., 2020).

proposed additional microplates in southern and eastern Africa (Victoria, Rovuma, and Lwandle) based on bands of earthquakes and active faults along edges of the cratons (Calais et al., 2006; Hartnady, 2002; Horner-Johnson et al., 2007; Stamps et al., 2008), as well as zones of diffuse deformation inconsistent with rigid plates (Stamps et al., 2020). However, the line of active rifts from southern Tanzania, through the Luangwa and Luano Rifts in Zambia and into the Okavango Rift in Botswana, known as the southwestern branch of the EARS (Figure 1a; Fairhead & Girdler, 1969; Scholz et al., 1976), is not accounted for in current kinematic models. Despite suggestions that southern Africa can be modeled with additional microplates (e.g., the San microplate in Daly et al., 2020), the plate motions for more complex configurations have not been constrained until now.

The southern Malawi Rift is located at the southern amagmatic end of the western branch of the EARS. The crust in the southern Malawi Rift is >40 km thick and has experienced a similar level of crustal thinning (2–3 km; Sun et al., 2021; Wang et al., 2019) as the rifts along the southwestern branch of the EARS (~2 km in the Luangwa Rift and ~5 km in the Okavango Rift; Wang et al., 2019; Yu et al., 2015). During the Quaternary, deformation has been distributed across multiple faults spanning ~50–100 km wide rift basins (Wedmore, Biggs, et al., 2020; Williams et al., 2021). Previous plate models estimate the extension rate across the center of the Malawi Rift ranges from 3.50 ± 0.29 mm/yr (Stamps et al., 2008) to 1.66 ± 1.70 mm/yr (Saria et al., 2013). The distribution of strain in southern Malawi is poorly known, as prior to this study there were only two GNSS stations in the region (Saria et al., 2014).

Here, we process new and existing GNSS data from southern Africa to explore plate configuration and strain distribution during amagmatic continental rifting in a region where unmodified lithosphere is ~150 km thick (Accardo et al., 2020; O'Donnell et al., 2013; Priestley et al., 2018) and crustal thinning is <10% (Njinju et al., 2019). First, we model GNSS velocities to explore a possible new three-plate configuration in southern Africa where the San microplate is separated from the Nubian and Rovuma plates. We then report on campaign GNSS surveys from the southern Malawi Rift to investigate the geodetic strain distribution and its relationship to the surface faulting and properties of the underlying lithosphere.

2. GNSS Surveys and Processing

We present new data from nine campaign GNSS sites that we established and surveyed in southern Malawi between 2016 and 2019. Each site has three or more occupations during this time and at least 3 years between the first and last occupation. Each occupation lasted between 2 and 12 days (average 4.9 days).

We processed our nine survey sites alongside 53 continuous and survey sites (see Data Sets S1 and S2 for list of data references), including all available sites that form a part of the International GNSS Service (IGS) network (www.igs.org), accessed from the NASA CDDIS data center (Noll, 2010). All data were processed using the GAMIT/GLOBK software (Herring et al., 2018) in a two-stage approach (e.g., McCaffrey et al., 2007; Reilinger et al., 2006), using IGS final orbits from CDDIS. We generated daily position time series that were visually inspected for discontinuities caused by documented or undocumented equipment changes or changes in site conditions. We added white noise to obvious outliers to ensure the formal uncertainty of such data points that did not increase the normalized RMS misfit of the time series (Data Set S5). We then combined daily position estimates into a single position solution for each survey (e.g., McCaffrey et al., 2007).

We used the software Hector (Bos et al., 2013) to calculate temporally correlated noise, assuming a white-plus-flicker noise model, in daily time series solutions from the Nevada Geodetic Laboratory (Blewitt et al., 2018) for continuous stations in our study (including discontinuities for earthquakes, equipment changes, and other transient motions). We applied the median temporally correlated noise value from the regional stations (converted to equivalent random walk magnitude e.g., Zhang et al., 1997) to our survey sites during the Kalman filter stage in GLOBK. This produced a single-velocity solution for the 4 years of the data in the ITRF2014 reference frame (Altamimi et al., 2017). We combined our southern Malawi velocity solution with the GeoPRISMS community geodetic solution (King et al., 2019) using the full solutions including associated covariance matrices. To expand the number of sites on the Nubian Plate, we aligned the velocity solution of Saria et al. (2014; after it had been rotated into the ITRF2014 reference frame using

Table 1
Euler Poles, Plate Angular Velocities (Positive is Anti-Clockwise Around the Euler Pole) and Geocentric Rotation Rate Vectors for the Two- and Three-Plate Models

	Angular velocity			Geocentric rotation rate vectors (deg/Myr)		
Plates	Lat (°)	Lon (°)	Ang (°/Myr)	*X*	*Y*	*Z*
Two-plate solution						
Nubia-ITRF2014	48.643 ± 0.067	−79.374 ± 0.242	0.266 ± 0.000	0.0324 ± 0.0007	−0.1729 ± 0.0004	0.1998 ± 0.0004
Rovuma-ITRF2014	47.221 ± 2.371	−96.650 ± 6.497	0.314 ± 0.023	−0.0247 ± 0.0269	−0.2116 ± 0.0223	0.2302 ± 0.0083
Rovuma-Nubia	−23.778 ± 5.030	34.134 ± 2.924	−0.075 ± 0.035	−0.0571 ± 0.0269	−0.0387 ± 0.0223	0.0304 ± 0.0083
Three-plate solution						
Nubia-ITRF2014	48.775 ± 0.099	−79.063 ± 0.430	0.266 ± 0.001	0.0332 ± 0.0013	−0.1720 ± 0.0005	0.1999 ± 0.0005
Rovuma-ITRF2014	47.221 ± 2.371	−96.650 ± 6.497	0.314 ± 0.023	−0.0247 ± 0.0269	−0.2116 ± 0.0223	0.2302 ± 0.0083
San-ITRF2014	49.244 ± 0.145	−84.566 ± 1.088	0.277 ± 0.002	0.0171 ± 0.0033	−0.1799 ± 0.0014	0.2097 ± 0.0022
Rovuma-Nubia	−23.373 ± 4.810	34.392 ± 2.806	−0.076 ± 0.0352	−0.0579 ± 0.0269	−0.0396 ± 0.0223	0.0303 ± 0.0083
San-Nubia	−28.622 ± 2.695	26.260 ± 2.465	−0.0205 ± 0.0043	−0.0161 ± 0.0036	−0.0080 ± 0.0015	0.0098 ± 0.0022
San-Rovuma	−21.369 ± 5.366	37.170 ± 2.273	0.0563 ± 0.0357	0.0418 ± 0.0271	0.0317 ± 0.0223	−0.0205 ± 0.0086

Note. For full variance and covariance information, see Data Sets S3 and S4.

parameters in Saria et al., 2013) with our combined southern Malawi-GeoPRISMS velocity solution, using a three-parameter rotation matrix to minimize the difference in velocities at 53 common sites (Data Set S1).

3. Determination and Definition of Plates

The ITRF2014 plate motion model uses nine stations in southern Africa to define the rigid Nubia Plate, but these stations have south-eastward trending velocity residuals (Figure 1d; Altamimi et al., 2017). We test whether dividing the Nubia Plate along the southwestern branch of the EARS (Daly et al., 2020; Figure 1d) can produce an angular velocity solution that removes these systematic residuals. We estimate the angular velocity solution by solving for a rotation rate vector per plate to minimize the horizontal GNSS velocities of a set of sites defining each plate (see Data Sets S3 and S4). Daly et al. (2020) also propose the existence of a triangular-shaped microplate known as Angoni, which is bordered by the Malawi Rift in the east, the Luangwa and Luano Rifts in the west, and the Lower Zambezi and Lower Shire Rifts in the south. We do not model the Angoni microplate due to a lack of suitable GNSS sites in this region. We also adjust the Rovuma-San boundary to follow the Urema and Mazenga grabens in Mozambique, which are characterized by instrumentally recorded seismicity, including the 2006 M_w7.0 Machaze earthquake and aftershock sequence, and the low upper-crustal shear-wave velocities (Copley et al., 2012; Domingues et al., 2016; Fonseca et al., 2014; Lloyd et al., 2019).

We tested the significance of a new three-plate configuration (Nubia, San, and Rovuma), relative to the traditional two-plate interpretation (Nubia and Rovuma; e.g., Calais et al., 2006; Saria et al., 2013; Stamps et al., 2008), using sites with horizontal velocity uncertainties of <1.5 mm/yr, located >150 km from a plate boundary, and excluding nearby redundant sites (Figure 1b). Previous definitions of Nubia used sites that were clustered in South Africa and north of the Gulf of Guinea, so we define a new subset of sites with a better geographic distribution. Our two-plate solution (Nubia-Rovuma) is based on 27 sites on the Nubian Plate (see Data Set S3) and for our three-plate solution (Nubia-Rovuma-San), seven of these lie on the San microplate (Figure 1b; Data Set S4).

In both the two- and three-plate models, the Nubia Euler pole (relative to ITRF2014) is consistent with previous estimates (Table 1). The WRMS for Nubia in our models (0.249 mm/yr—two-plate and 0.246 mm/yr—three-plate) is less than previous definitions of Nubia (0.6 mm/yr—Saria et al., 2013 and 0.5 mm/yr—Saria et al., 2014). The weighted mean residual of the GNSS velocities for the seven San sites is 0.17 mm/yr, significantly less than the weighted mean residual of the sites in southern Africa within previous definitions of stable Nubia (1.3 mm/yr—Saria et al., 2013; 6.2 mm/yr—Saria et al., 2014; and 0.56 mm/yr—Altamimi

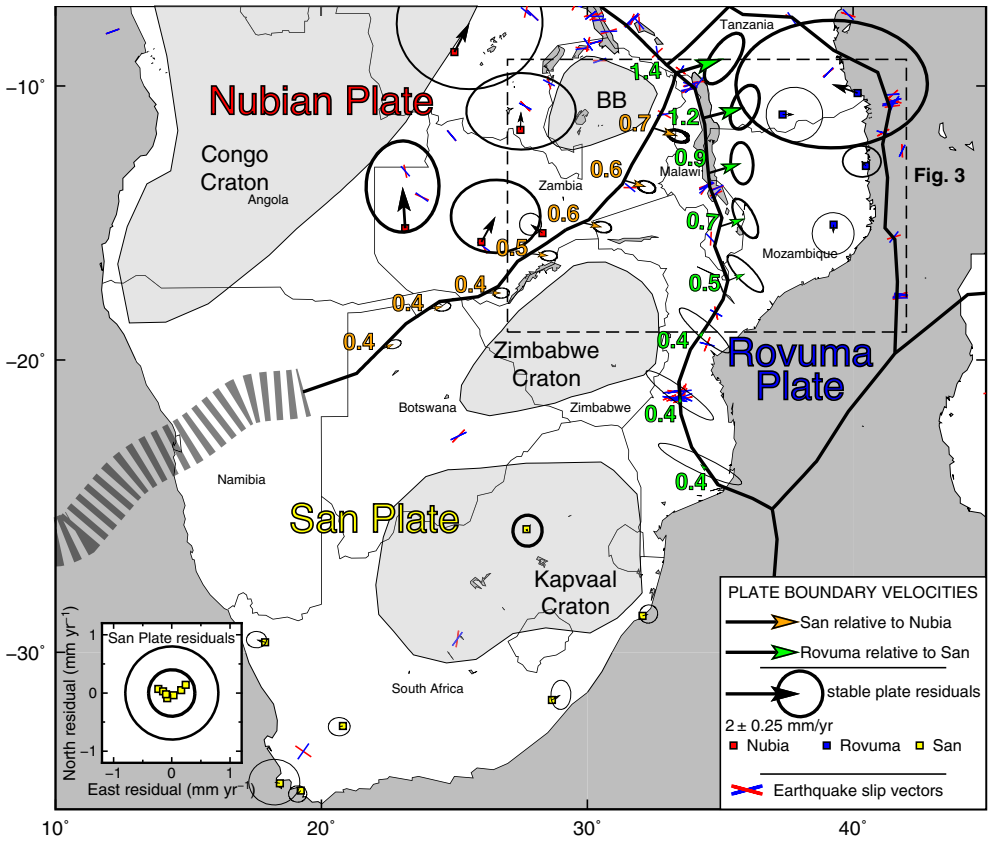

Figure 2. Plate boundary velocities in southern Africa. The colored arrows show the velocity along the plate boundaries predicted by our solution and the 1-sigma uncertainties, with the magnitude of the velocity in numbers. Gray arrows show the residual velocities of the sites used to define the plate angular velocities (relative to each plate) and associated 2-sigma uncertainties. Inset is the residual velocities for sites on the San microplate. Earthquake slip vectors are from focal mechanisms in Craig et al. (2011) and Craig and Jackson (2021). BB, Bangweulu Block.

et al., 2017). The San microplate rotates clockwise relative to Nubia, with the Euler pole located near the center of South Africa (Table 1; Figure 1b). The Rovuma microplate rotates clockwise relative to Nubia, with the pole located in southern Mozambique (Figures 1b and S1; Table 1), to the south of the pole identified by Saria et al. (2013) but within their 95% confidence ellipse (Figure S1). The Rovuma microplate rotates clockwise relative to San, with a pole located off the southern coast of Mozambique (Figure 1b).

Our three-plate model finds extension rates of 0.7 ± 0.3 mm/yr across the Luangwa Rift, 0.6 ± 0.2 mm/yr across the Luano Rift, 0.4 ± 0.2 mm/yr across the Okavango Rift, and 0.7 ± 0.2 mm/yr across the southern Malawi Rift (Figures 1a and 2). Across the Urema (0.4 ± 0.5 mm/yr) and Mazenga grabens (0.4 ± 0.8 mm/yr), 1-sigma uncertainties are larger than the extension rates implied by our solution (Figures 1a and 2).

The residual velocities on the San microplate have no systematic pattern (inset in Figure 2), unlike the SE-trending velocity residuals of southern African sites on Nubia in ITRF2014 (Figure 1a; Altamimi et al., 2017). The chi-squared misfit is 109.6 for the two-plate solution and 82.4 for the three-plate solution. The calculated F-statistic (Stein & Gordon, 1984) for the two- versus three-plate solution is 9.26, which is above the 99% confidence level of 4.0. Therefore, our three-plate solution is a statistically significant improvement at a >99% confidence level.

4. Distributed Extension Across the Southern Malawi Rift

We use the sites we established and surveyed in southern Malawi to investigate the kinematics of rifting in the region across the Nubia, San, and Rovuma plates (Figure 3). Eight of our sites have horizontal velocity uncertainties <1.5 mm/yr, of which seven have velocities larger than their 1-sigma uncertainties, and five

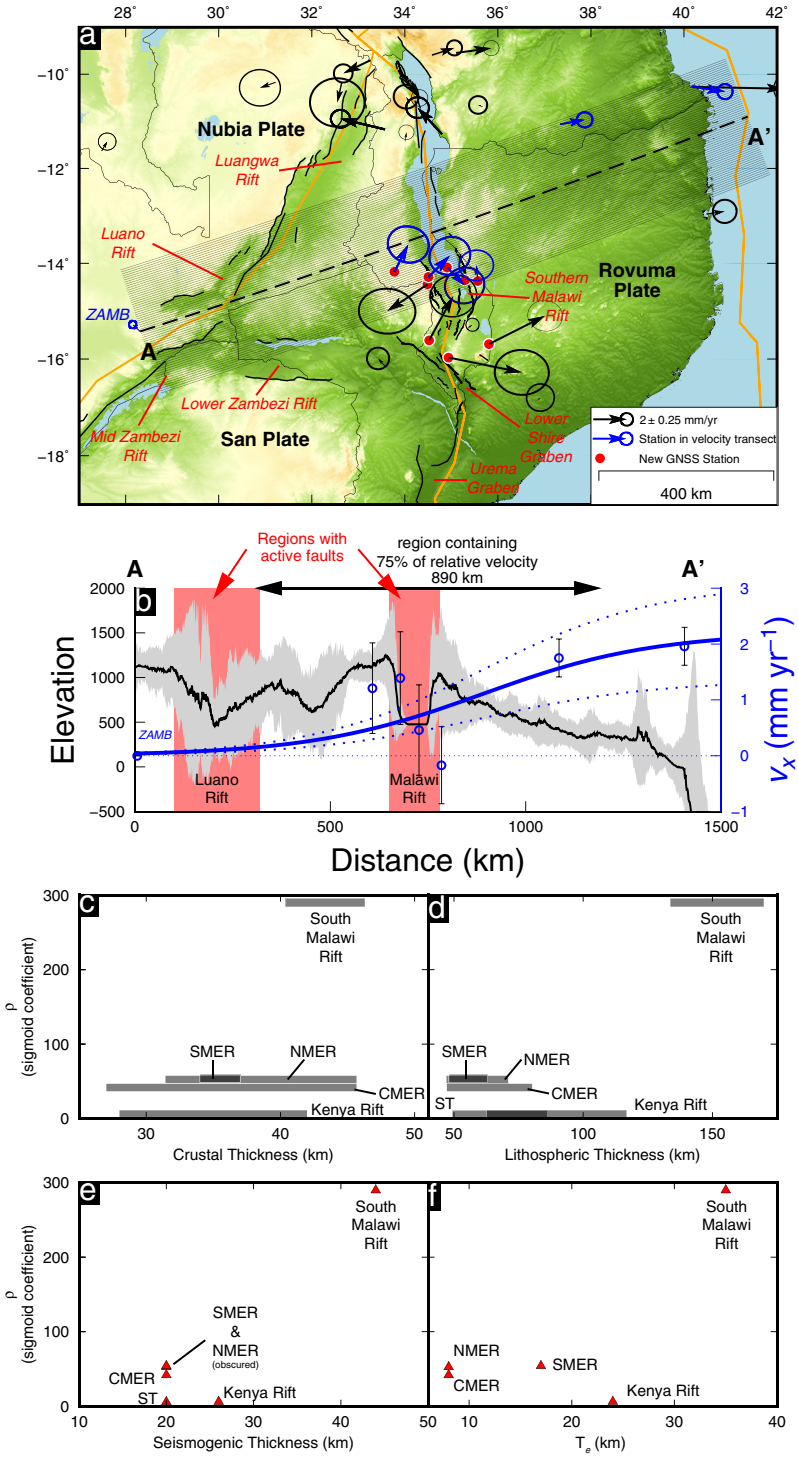

Figure 3. Global Positioning System (GPS) velocities recorded across the southern East African Rift System. (a) GPS velocities plotted relative to stable San microplate with 1-sigma errors. Faults (black lines) are from Williams et al. (2021) and Daly et al. (2020). (b) GPS velocities relative to the site ZAMB (see part a) in blue, fit with a sigmoid function (blue line) and 2-sigma uncertainties (dotted line). $v_{\min}$ has been fixed at 0 to ensure that ZAMB has zero velocity in the best-fit sigmoid profile. The black line shows median swath topography across the transect (maximum and minimum values are shaded). (c–f) The sigmoid coefficient, ρ, from the southern Malawi Rift velocity profile and five other Global Navigation Satellite System (GNSS) transects across the EARS previously fitted with a sigmoid function (Knappe et al., 2020; Kogan et al., 2012) plotted against (c) the range of the lithospheric thickness, (d) crustal thickness, (e) seismogenic thickness, and (f) effective elastic thickness (T_e) in each region (see Table S1 for details of the measurements). CMER, central Main Ethiopian Rift; NMER, northern Main Ethiopian Rift; SMER, southern Main Ethiopian Rift; and ST, southern Turkana Rift.

display NE-E extension relative to the site ZAMB and IGS sites on the Nubia Plate operating since 2002 (Figure 3a). We project the magnitude of the velocity vectors relative to ZAMB onto a 1,500 km long profile parallel to the direction of minimum compressive stress in southern Malawi (072 ± 14°; Williams et al., 2019). We exclude sites with uncertainty >1.5 mm/yr, site NJON, which has an anomalous south-westerly motion, and the three sites below −15° latitude due to the complex changes in fault strike in this region.

We compare the distribution of strain in the southern Malawi Rift with that of five other EARS rifts that have previously been analyzed (Figures 3c–3e; Table S1; Knappe et al., 2020; Kogan et al., 2012) by fitting a sigmoid function (Kogan et al., 2012) to the velocity data along our profile:

$$v_x = v_{\min} + \frac{v_{\max}}{1 + \exp\left(\frac{x_0 - x}{\rho}\right)} \quad (1)$$

where v_x is the velocity, $v_{\min}$ is the minimum velocity, $v_{\max}$ is the maximum velocity, x_0 is the point of inflection of the sigmoid, and ρ is the sigmoid rate coefficient, which is related to the width of the straining region. The spatial derivative of the sigmoid approximates the strain rate. The best-fit sigmoid function for the southern Malawi Rift has an extension rate ($v_{\max}$) of 2.2 ± 0.3 mm/yr (standard error; $v_{\min}$ is fixed to zero), a maximum strain rate of 1.9×10^{-9} yr^{-1}, and a ρ of 290 (Figure 3b). This equates to an 890 km wide region that contains 75% of the relative velocity (Figure 3b). The value for ρ from our profile is ∼5–60 times higher than that of previously published profiles across the magmatic sections of the EARS (Figures 3c and 3d; Table S1; Knappe et al., 2020; Kogan et al., 2012).

5. Discussion

5.1. Three-Plate Model

The kinematic model of southern Africa presented here is the first geodetic model to account for the faulting and seismicity along the southwestern branch of the EARS. Previous geodetic solutions found no statistical difference between the motion of GNSS sites in southern and northern Nubia (Calais et al., 2006; Saria et al., 2013). With a longer time series now available, we show that our three-plate solution, where Nubia is subdivided into Nubia and San, fits the GNSS data better at a 99% confidence level. This configuration is supported by observations of active faulting along the San-Nubia and San-Rovuma boundaries (Daly et al., 2020; Kinabo et al., 2008; Wedmore, Williams, et al., 2020), which run along the edges of the Congo, Zimbabwe, and Kapvaal cratons and the Bangweulu block (Figure 2). We have insufficient data to model the Angoni microplate, which has been proposed to further subdivide the San microplate (Daly et al., 2020), along a line of active faults in the Lower Zambezi Rift (Mackintosh et al., 2019; Figure 1).

Extension rates along the San-Nubia boundary decrease from ∼0.7 mm/yr across the Luangwa and Luano Rifts to ∼0.4 mm/yr across the Okavango Rift, one of the youngest EARS basins (Figure 2; Kinabo et al., 2008; Modisi et al., 2000; Scholz et al., 1976). Our model implies E-W to NE-SW motion of San relative to Nubia, which is oblique to the NE-SW strike of normal faults in the rift basins in the southwestern EARS. Our results disagree with a previous suggestion that faults in the rift accommodate pure strike-slip motion (Pastier et al., 2017), but are similar to the southern Malawi Rift, where reactivated faults strike oblique to the direction of least compressive stress (Williams et al., 2019). Like other purely geodetic studies (e.g., Saria et al., 2013), our model is poorly constrained in southern Mozambique (Figure 2), but models that also incorporate earthquakes slip vectors and spreading rates suggest extension (Saria et al., 2014; Stamps et al., 2008), consistent with focal mechanisms from the Machaze-Zinave earthquake sequence (Copley et al., 2012; Lloyd et al., 2019).

5.2. Strain Distribution

Our velocity profile encompasses two distinct <∼150 km wide zones of active faulting—the Luangwa-Luano and the southern Malawi Rifts. There are no observations of aseismic creep or $M_w > 6.5$ earthquakes in this region during the last century, so we assume that the velocities reflect interseismic elastic strain accumulation. In contrast to the narrow (<150 km wide) bands of active faults, our profile shows that 75% of the relative motion is distributed within an 890 km wide region (Figure 3b). The center of the straining region,

x_0, is located over the southern Malawi Rift. This reflects either a lower extension rate or a lack of stations both in the near-field to the Luangwa-Luano Rifts and between the Luangwa-Luano and southern Malawi Rifts (Figure 3b). Thus, in southern Malawi, the relatively narrow zones of faulting and seismicity observed at the surface do not reflect the broad zone of interseismic strain that is accumulating at depth.

The extension rate across our profile of 2.2 ± 0.3 mm/yr (Figure 3b) is greater than the combined rates of our Nubia-San (0.6 ± 0.2 mm/yr) and San-Rovuma (0.7 ± 0.2 mm/yr) plate models. This difference could be because the broad straining region extends beyond the zone of active faulting (Figure 3b), meaning GPS stations on the Rovuma microplate (~300 km from the boundary) are not sufficiently far from the plate boundary to be considered as a part of the rigid plate interior. Thus, although plates are normally considered rigid if they accumulate <1 mm/yr of elastic strain (Argus & Gordon, 1996), this may not be sufficient in regions of low extension rate and broadly distributed strain. Consequently, the Rovuma-San Euler pole may lie closer to the Rovuma plate than our model suggests and/or the angular rotation rate for Rovuma may be an underestimate.

Our velocity profile of the southern Malawi Rift is the first to cross an amagmatic section of the western branch of the EARS, with unusually thick lithosphere (130–180 km; Priestley et al., 2018) and elevated topography (500–1,000 m asl; Figure 3b). For each of the six velocity profiles across the EARS (see Table S1), we compile the range of the lithospheric thickness along each profile from surface-wave tomography (Priestley et al., 2018; Figure S2), the range of crustal thickness along each profile from receiver function studies (Dugda et al., 2005; Ebinger et al., 2017; Stuart et al., 2006; Sun et al., 2021; Tugume et al., 2012; Wölbern et al., 2010; see Figure S3), the seismogenic thickness, defined as the maximum depth of upper crustal seismicity beneath each profile (Craig & Jackson, 2021; Ibs-von Seht et al., 2001; Keir et al., 2006), and the effective elastic thickness, measured using the coherence method (Ebinger & Hayward, 1996; Ebinger et al., 1999).

The ρ of the sigmoid fit in southern Malawi is ~5–60 times larger than the velocity profiles across the magmatic eastern branch of the EARS (Knappe et al., 2020; Kogan et al., 2012; Figure 3; Table S1). The relatively broad region of geodetically determined strain across the southern Malawi Rift may relate to anomalously thick lithosphere (130–170 km; Figures 3c–3f). Despite evidence for lateral heterogeneities localizing permanent strain near the surface (Hodge et al., 2018; Wedmore, Williams, et al., 2020), the southern Malawi Rift has a strong, dry crust (Hellebrekers et al., 2019), and seismicity down to the Moho (Craig et al., 2011; Sun et al., 2021). The maximum crustal thickness in southern Malawi is comparable to the other EARS profiles considered here (Figure 3c), but estimates of the depth of seismicity (Figure 3e) and effective elastic thickness (Figure 3f) are much higher (Craig et al., 2011; Ebinger et al., 1999). Larger elastic thicknesses smooth lower-crustal strain, causing a broader pattern of strain at the surface (Turcotte & Schubert, 2002). However, when modeling the extension resulting from slip at depth on a single dipping dislocation, an increase in the elastic lid thickness from 20 to 44 km (assuming it is equivalent to seismogenic thickness; Figure 3e) only increases ρ by a factor of ~2 (Figure S4), much less than the 5–60 times increase we observe. Numerical models shows that lithospheric strength contrasts can decouple the crust and mantle lithosphere, leading to a wider region of deformation below the upper crust (Huismans & Beaumont, 2007). Low mid-crustal shear wave velocities (20–28 km depth; Wang et al., 2019) raise a hypothesis that small melt fractions may facilitate crust-mantle decoupling. Alternatively, the straining regions in the magmatic eastern branch of the EARS may be abnormally narrow. Each of the five other profiles have experienced shallow magmatic intrusions, and fluids from the upwelling asthenosphere that may have entered the thinned lithosphere, weakened the crust and thus caused localized deformation there (Ebinger & Casey, 2001).

6. Conclusions and Implications

Our new geodetic constraints demonstrate that southern Africa is not a part of a single rigid Nubian Plate, and that interseismic strain is more broadly distributed than suggested by faulting and seismicity in the upper crust. Extension rates across the southwestern branch of the EARS, which divides the San and Nubian plates, are 0.4–0.7 mm/yr. This boundary follows the edges of the Proterozoic-age Congo and Zimbabwe cratons and the Bangweulu block, which are rigid relative to the surrounding metamorphic belts that consist of weaker and inherited lithosphere (Katz, 1985; McKenzie & Priestley, 2008). Other cratons may also

behave as separate microplates: the 2017 M_w6.5 Moiyabana earthquake in Botswana reactivated fabrics in the Limpopo-Shashe orogenic belt between the Kaapvaal and Zimbabwe cratons (Gardonio et al., 2018; Kolawole et al., 2017; Midzi et al., 2018), and there is heightened seismic activity in the Lake Mweru Rift at the edge of the Bangweulu Block. As the number of GNSS stations and the length of occupation increases, an increasing number of microplates or a continuum model may be required to describe the kinematics of southern Africa.

Data Availability Statement

All new GNSS data presented in this manuscript are available on the Unavco data archive at https://doi.org/10.7283/FASE-5453. Our velocity solution is available in the supporting information and on the Zenodo data repository at https://doi.org/10.5281/zenodo.5031366.

Acknowledgments
The authors thank Kondwani Dombola, Denson Makwela, and Jalf Salima at the Geological Survey Department, Malawi for making this work possible. The authors also thank the district governors, drivers, schoolteachers, doctors, national park wardens, and guards in Malawi for assistance with the GPS deployment. We thank Ophelia George for her assistance in uploading the GNSS data to Unavco. The authors thank the Cindy Ebinger, two other reviewers, and the associate editor for careful and detailed comments that significantly improved this manuscript. This work was funded by a number of EPSRC grants funded under the Global Challenges Research Fund (GCRF): PREPARE (EP/P028233/1); SAFER PREPARED (part of the "Innovative data services for aquaculture, seismic resilience, and drought adaptation in East Africa" grant; EP/T015462/1); and a GCRF EPSRC Institutional Sponsorship Award. The authors also received a fieldwork grant from COMET, the NERC Centre for the Observation and Modeling of Earthquakes, Volcanoes, and Tectonics, a partnership between UK Universities and the British Geological Survey. This material is based on services provided by the GAGE Facility, operated by UNAVCO, Inc., with the support from the National Science Foundation and the National Aeronautics and Space Administration under NSF Cooperative Agreement EAR-1724794.

References

Accardo, N. J., Gaherty, J. B., Shillington, D. J., Hopper, E., Nyblade, A. A., Ebinger, C. J., et al. (2020). Thermochemical modification of the upper mantle beneath the northern Malawi Rift constrained from shear velocity imaging. *Geochemistry, Geophysics, Geosystems*, *21*, 1–19. https://doi.org/10.1029/2019GC008843

Altamimi, Z., Métivier, L., Rebischung, P., Rouby, H., & Collilieux, X. (2017). ITRF2014 plate motion model. *Geophysical Journal International*, *209*, 1906–1912. https://doi.org/10.1093/gji/ggx136

Argus, D. F., & Gordon, R. G. (1996). Tests of the rigid-plate hypothesis and bounds on intraplate deformation using geodetic data from very long baseline interferometry. *Journal of Geophysical Research*, *101*, 13555–13572. https://doi.org/10.1029/95JB03775

Becker, J. J., Sandwell, D. T., Smith, W. H. F., Braud, J., Binder, B., Depner, J., et al. (2009). Global bathymetry and elevation data at 30 arc seconds resolution: SRTM30_PLUS. *Marine Geodesy*, *32*, 355–371. https://doi.org/10.1080/01490410903297766

Blewitt, G., Hammond, W., & Kreemer, C. (2018). Harnessing the GPS data explosion for Interdisciplinary Science. *Eos*, *99*. https://doi.org/10.1029/2018EO104623

Bos, M. S., Fernandes, R. M. S., Williams, S. D. P., & Bastos, L. (2013). Fast error analysis of continuous GNSS observations with missing data. *Journal of Geodesy*, *87*, 351–360. https://doi.org/10.1007/s00190-012-0605-0

Calais, E., Ebinger, C., Hartnady, C., & Nocquet, J. M. (2006). Kinematics of the East African Rift from GPS and earthquake slip vector data. *Geological Society, London, Special Publications*, *259*, 9–22. https://doi.org/10.1144/GSL.SP.2006.259.01.03

Copley, A., Hollingsworth, J., & Bergman, E. (2012). Constraints on fault and lithosphere rheology from the coseismic slip and postseismic afterslip of the 2006 M_w7.0 Mozambique earthquake. *Journal of Geophysical Research*, *117*. https://doi.org/10.1029/2011JB008580

Corti, G. (2009). Continental rift evolution: From rift initiation to incipient break-up in the Main Ethiopian Rift, East Africa. *Earth-Science Reviews*, *96*, 1–53. https://doi.org/10.1016/j.earscirev.2009.06.005

Craig, T. J., & Jackson, J. A. (2021). Variations in the seismogenic thickness of East Africa. *Journal of Geophysical Research: Solid Earth*, *126*. https://doi.org/10.1029/2020JB020754

Craig, T. J., Jackson, J. A., Priestley, K., & Mckenzie, D. (2011). Earthquake distribution patterns in Africa: Their relationship to variations in lithospheric and geological structure, and their rheological implications. *Geophysical Journal International*, *185*, 403–434. https://doi.org/10.1111/j.1365-246X.2011.04950.x

Daly, M. C., Chorowicz, J., & Fairhead, J. D. (1989). Rift basin evolution in Africa: The influence of reactivated steep basement shear zones. *Geological Society, London, Special Publications*, *44*, 309–334. https://doi.org/10.1144/GSL.SP.1989.044.01.17

Daly, M. C., Green, P., Watts, A. B., Davies, O., Chibesakunda, F., & Walker, R. (2020). Tectonics and landscape of the Central African Plateau, and their implications for a propagating Southwestern Rift in Africa. *Geochemistry, Geophysics, Geosystems*, *21*, e2019GC008746. https://doi.org/10.1029/2019GC008746

Domingues, A., Silveira, G., Ferreira, A. M. G., Chang, S. J., Custodio, S., & Fonseca, J. F. B. D. (2016). Ambient noise tomography of the East African Rift in Mozambique. *Geophysical Journal International*, *204*, 1565–1578. https://doi.org/10.1093/gji/ggv538

Dugda, M. T., Nyblade, A. A., Julia, J., Langston, C. A., Ammon, C. J., & Simiyu, S. (2005). Crustal structure in Ethiopia and Kenya from receiver function analysis: Implications for rift development in eastern Africa. *Journal of Geophysical Research*, *110*. https://doi.org/10.1029/2004JB003065

Ebinger, C. J. (2005). Continental break-up: The East African perspective. *Astronomy and Geophysics*, *46*, 2.16–2.21. https://doi.org/10.1111/j.1468-4004.2005.46216.x

Ebinger, C. J., & Casey, M. (2001). Continental breakup in magmatic provinces: An Ethiopian example. *Geology*, *29*, 527–530. https://doi.org/10.1130/0091-7613(2001)029<0527:CBIMPA>2.0.CO;2

Ebinger, C. J., & Hayward, N. J. (1996). Soft plates and hot spots: Views from Afar. *Journal of Geophysical Research*, *101*, 21859–21876. https://doi.org/10.1029/96JB02118

Ebinger, C. J., Jackson, J. A., Foster, A. N., & Hayward, N. J. (1999). Extensional basin geometry and the elastic lithosphere. *Philosophical Transactions of the Royal Society A: Mathematical, Physical & Engineering Sciences*, *357*, 741–765. https://doi.org/10.1098/rsta.1999.0351

Ebinger, C. J., Keir, D., Bastow, I. D., Whaler, K., Hammond, J. O. S., Ayele, A., et al. (2017). Crustal structure of active deformation zones in Africa: Implications for global crustal processes. *Tectonics*, *36*, 3298–3332. https://doi.org/10.1002/2017TC004526

Ebinger, C. J., Oliva, S. J., Pham, T. Q., Peterson, K., Chindandali, P., Illsley-Kemp, F., et al. (2019). Kinematics of active deformation in the Malawi Rift and Rungwe Volcanic Province, Africa. *Geochemistry, Geophysics, Geosystems*, *20*, 3928–3951. https://doi.org/10.1029/2019GC008354

Fairhead, J. D., & Girdler, R. W. (1969). How far does the rift system extend through Africa? *Nature*, *221*, 1018–1020. https://doi.org/10.1038/2211018a0

Fernandes, R. M. S., Ambrosius, B. A. C., Noomen, R., Bastos, L., Combrinck, L., Miranda, J. M., & Spakman, W. (2004). Angular velocities of Nubia and Somalia from continuous GPS data: Implications on present-day relative kinematics. *Earth and Planetary Science Letters*, *222*, 197–208. https://doi.org/10.1016/j.epsl.2004.02.008

Fonseca, J. F. B. D., Chamussa, J., Domingues, A., Helffrich, G., Antunes, E., Van Aswegen, G., et al. (2014). MOZART: A seismological investigation of the East African Rift in central Mozambique. *Seismological Research Letters*, *85*, 108–116. https://doi.org/10.1785/0220130082

Gardonio, B., Jolivet, R., Calais, E., & Leclère, H. (2018). The April 2017 M_w6.5 Botswana earthquake: An intraplate event triggered by deep fluids. *Geophysical Research Letters*, *45*, 8886–8896. https://doi.org/10.1029/2018GL078297

Hartnady, C. J. H. (2002). Earthquake hazard in Africa: Perspectives on the Nubia-Somalia boundary. *South African Journal of Science*, *98*, 425–428.

Hellebrekers, N., Niemeijer, A. R., Fagereng, Å., Manda, B., & Mvula, R. L. S. (2019). Lower crustal earthquakes in the East African Rift System: Insights from frictional properties of rock samples from the Malawi Rift. *Tectonophysics*, *767*, 228167. https://doi.org/10.1016/j.tecto.2019.228167

Herring, T. A., King, R. W., Floyd, M. A., & McClusky, S. C. (2018). *Introduction to GAMIT/GLOBK: Release 10.7* (p. 54). Masschusetts Institute of Technology.

Hodge, M., Fagereng, Å., Biggs, J., & Mdala, H. (2018). Controls on early-rift geometry: New perspectives from the Bilila-Mtakataka Fault, Malawi. *Geophysical Research Letters*, *45*, 3896–3905. https://doi.org/10.1029/2018GL077343

Horner-Johnson, B. C., Gordon, R. G., & Argus, D. F. (2007). Plate kinematic evidence for the existence of a distinct plate between the Nubian and Somalian plates along the Southwest Indian Ridge. *Journal of Geophysical Research*, *112*. https://doi.org/10.1029/2006JB004519

Huismans, R. S., & Beaumont, C. (2007). Roles of lithospheric strain softening and heterogeneity in determining the geometry of rifts and continental margins. *Geological Society, London, Special Publications*, *282*, 111–138. https://doi.org/10.1144/SP282.6

Ibs-von Seht, M., Blumenstein, S., Wagner, R., Hollnack, D., & Wohlenberg, J. (2001). Seismicity, seismotectonics and crustal structure of the southern Kenya Rift—New data from the Lake Magadi area. *Geophysical Journal International*, *146*, 439–453. https://doi.org/10.1046/j.0956-540x.2001.01464.x

Jestin, F., Huchon, P., & Gaulier, J. M. (1994). The Somalia plate and the East African Rift System: Present-day kinematics. *Geophysical Journal International*, *116*, 637–654. https://doi.org/10.1111/j.1365-246X.1994.tb03286.x

Katz, M. B. (1985). The tectonics of Precambrian craton-mobile belts: Progressive deformation of polygonal miniplates. *Precambrian Research*, *27*, 307–319. https://doi.org/10.1016/0301-9268(85)90091-9

Keir, D., Ebinger, C. J., Stuart, G. W., Daly, E., & Ayele, A. (2006). Strain accommodation by magmatism and faulting as rifting proceeds to breakup: Seismicity of the northern Ethiopian Rift. *Journal of Geophysical Research*, *111*. https://doi.org/10.1029/2005JB003748

Kendall, J.-M., & Lithgow-Bertelloni, C. (2016). Why is Africa rifting? *Geological Society, London, Special Publications*, *420*, 11–30. https://doi.org/10.1144/SP420.17

Kinabo, B. D., Hogan, J. P., Atekwana, E. A., Abdelsalam, M. G., & Modisi, M. P. (2008). Fault growth and propagation during incipient continental rifting: Insight from a combined aeromagnetic and Shuttle Radar Topography Mission digital elevation model investigation of the Okavango Rift Zone, northwest Botswana. *Tectonics*, *27*, 1–16. https://doi.org/10.1029/2007TC002154

King, R., Floyd, M., Reilinger, R., & Bendick, R. (2019). *GPS velocity field (MIT 2019.0) for the East African Rift System generated by King et al*. Interdisciplinary Earth Data Alliance (IEDA). https://doi.org/10.1594/IEDA/324785

Knappe, E., Bendick, R., Ebinger, C., Birhanu, Y., Lewi, E., Floyd, M., et al. (2020). Accommodation of East African Rifting across the Turkana depression. *Journal of Geophysical Research: Solid Earth*, *125*, 1–13. https://doi.org/10.1029/2019JB018469

Kogan, L., Fisseha, S., Bendick, R., Reilinger, R., McClusky, S., King, R., & Solomon, T. (2012). Lithospheric strength and strain localization in continental extension from observations of the East African Rift. *Journal of Geophysical Research*, *117*. https://doi.org/10.1029/2011JB008516

Kolawole, F., Atekwana, E. A., Malloy, S., Stamps, D. S., Grandin, R., Abdelsalam, M. G., et al. (2017). Aeromagnetic, gravity, and Differential Interferometric Synthetic Aperture Radar analyses reveal the causative fault of the 3 April 2017 M_w 6.5 Moiyabana, Botswana, earthquake. *Geophysical Research Letters*, *44*, 8837–8846. https://doi.org/10.1002/2017GL074620

Lavayssière, A., Drooff, C., Ebinger, C., Gallacher, R., Illsley-Kemp, F., Oliva, S. J., & Keir, D. (2019). Depth extent and kinematics of faulting in the Southern Tanganyika Rift. *Africa: Tectonics*, *38*, 842–862. https://doi.org/10.1029/2018TC005379

Lloyd, R., Biggs, J., & Copley, A. (2019). The decade-long Machaze-Zinave aftershock sequence in the slowly straining Mozambique Rift. *Geophysical Journal International*, *217*, 504–531. https://doi.org/10.1093/gji/ggz033

Mackintosh, V., Kohn, B., Gleadow, A., & Gallagher, K. (2019). Long-term reactivation and morphotectonic history of the Zambezi Belt, northern Zimbabwe, revealed by multi-method thermochronometry. *Tectonophysics*, *750*, 117–136. https://doi.org/10.1016/j.tecto.2018.11.009

Manzunzu, B., Midzi, V., Mulabisana, T. F., Zulu, B., Pule, T., Myendeki, S., & Rathod, G. W. (2019). Seismotectonics of South Africa. *Journal of African Earth Sciences*, *149*, 271–279. https://doi.org/10.1016/j.jafrearsci.2018.08.012

McCaffrey, R., Qamar, A. I., King, R. W., Wells, R., Khazaradze, G., Williams, C. A., et al. (2007). Fault locking, block rotation and crustal deformation in the Pacific Northwest. *Geophysical Journal International*, *169*, 1315–1340. https://doi.org/10.1111/j.1365-246X.2007.03371.x

McKenzie, D., & Priestley, K. (2008). The influence of lithospheric thickness variations on continental evolution. *Lithos*, *102*, 1–11. https://doi.org/10.1016/j.lithos.2007.05.005

Midzi, V., Saunders, I., Manzunzu, B., Kwadiba, M. T., Jele, V., Mantsha, R., et al. (2018). The 03 April 2017 Botswana M6.5 earthquake: Preliminary results. *Journal of African Earth Sciences*, *143*, 187–194. https://doi.org/10.1016/j.jafrearsci.2018.03.027

Modisi, M. P., Atekwana, E. A., Kampunzu, A. B., & Ngwisanyi, T. H. (2000). Rift kinematics during the incipient stages of continental extension: Evidence the nascent Okavango rift basin. *Northwest Botswana: Geology*, *28*, 939–942. https://doi.org/10.1130/0091-7613(2000)028<0939:rkdtis>2.3.co;2

Njinju, E. A., Atekwana, E. A., Stamps, D. S., Abdelsalam, M. G., Atekwana, E. A., Mickus, K. L., et al. (2019). Lithospheric structure of the Malawi Rift: Implications for magma-poor rifting processes. *Tectonics*, *38*, 3835–3853. https://doi.org/10.1029/2019TC005549

Noll, C. E. (2010). The crustal dynamics data information system: A resource to support scientific analysis using space geodesy. *Advances in Space Research*, *45*, 1421–1440. https://doi.org/10.1016/j.asr.2010.01.018

O'Donnell, J. P., Adams, A., Nyblade, A. A., Mulibo, G. D., & Tugume, F. (2013). The uppermost mantle shear wave velocity structure of Eastern Africa from Raleigh wave tomography: Constraints on rift evolution. *Geophysical Journal International*, *194*, 961–978. https://doi.org/10.1093/gji/ggt135

Pastier, A.-M., Dauteuil, O., Murray-Hudson, M., Moreau, F., Walpersdorf, A., & Makati, K. (2017). Is the Okavango Delta the terminus of the East African Rift System? Towards a new geodynamic model: Geodetic study and geophysical review. *Tectonophysics*, *712–713*, 469–481. https://doi.org/10.1016/j.tecto.2017.05.035

Priestley, K., McKenzie, D., & Ho, T. (2018). A lithosphere-asthenosphere boundary—A global model derived from multimode surface-wave tomography and petrology. In H. Yuan & B. Romanowicz (Eds.), *Lithospheric discontinuities* (pp. 111–123). https://doi.org/10.1002/9781119249740.ch6

Reilinger, R., McClusky, S., Vernant, P., Lawrence, S., Ergintav, S., Cakmak, R., et al. (2006). GPS constraints on continental deformation in the Africa-Arabia-Eurasia continental collision zone and implications for the dynamics of plate interactions. *Journal of Geophysical Research*, *111*. https://doi.org/10.1029/2005JB004051

Saria, E., Calais, E., Altamimi, Z., Willis, P., & Farah, H. (2013). A new velocity field for Africa from combined GPS and DORIS space geodetic Solutions: Contribution to the definition of the African reference frame (AFREF). *Journal of Geophysical Research: Solid Earth*, *118*, 1677–1697. https://doi.org/10.1002/jgrb.50137

Saria, E., Calais, E., Stamps, D. S., Delvaux, D., & Hartnady, C. J. H. (2014). Present-day kinematics of the East African Rift. *Journal of Geophysical Research: Solid Earth*, *119*, 3584–3600. https://doi.org/10.1002/2013JB010901

Scholz, C. H., Koczynski, T. A., & Hutchins, D. G. (1976). Evidence for incipient rifting in Southern Africa. *Geophysical Journal of the Royal Astronomical Society*, *44*, 135–144. https://doi.org/10.1111/j.1365-246X.1976.tb00278.x

Stamps, D. S., Calais, E., Saria, E., Hartnady, C., Nocquet, J. M., Ebinger, C. J., & Fernandes, R. M. (2008). A kinematic model for the East African Rift. *Geophysical Research Letters*, *35*, 1–6. https://doi.org/10.1029/2007GL032781

Stamps, D. S., Kreemer, C., Fernandes, R., Rajaonarison, T. A., & Rambolamanana, G. (2020). Redefining East African Rift System kinematics. *Geology*, *49*, 150–155. https://doi.org/10.1130/G47985.1

Stein, S., & Gordon, R. G. (1984). Statistical tests of additional plate boundaries from plate motion inversions. *Earth and Planetary Science Letters*, *69*, 401–412. https://doi.org/10.1016/0012-821X(84)90198-5

Stuart, G. W., Bastow, I. D., & Ebinger, C. J. (2006). Crustal structure of the northern Main Ethiopian Rift from receiver function studies. *Geological Society, London, Special Publications*, *259*, 253–267. https://doi.org/10.1144/GSL.SP.2006.259.01.20

Sun, M., Gao, S. S., Liu, K. H., Mickus, K., Fu, X., & Yu, Y. (2021). Receiver function investigation of crustal structure in the Malawi and Luangwa rift zones and adjacent areas. *Gondwana Research*, *89*, 168–176. https://doi.org/10.1016/j.gr.2020.08.015

Tugume, F., Nyblade, A., & Julià, J. (2012). Moho depths and Poisson's ratios of Precambrian crust in East Africa: Evidence for similarities in Archean and Proterozoic crustal structure. *Earth and Planetary Science Letters*, *355–356*, 73–81. https://doi.org/10.1016/j.epsl.2012.08.041

Turcotte, D. L., & Schubert, G. (2002). *Geodynamics* (p. 607). Cambridge University Press.

Van Hinsbergen, D. J. J., Buiter, S. J. H., Torsvik, T. H., Gaina, C., & Webb, S. J. (2011). The formation and evolution of Africa from the Archaean to Present: Introduction. *Geological Society, London, Special Publications*, *357*, 1–8. https://doi.org/10.1144/SP357.1

Wang, T., Feng, J., Liu, K. H., & Gao, S. S. (2019). Crustal structure beneath the Malawi and Luangwa rift zones and adjacent areas from ambient noise tomography. *Gondwana Research*, *67*, 187–198. https://doi.org/10.1016/j.gr.2018.10.018

Wedmore, L. N. J., Biggs, J., Williams, J. N., Fagereng, Å., Dulanya, Z., Mphepo, F., & Mdala, H. (2020). Active fault scarps in Southern Malawi and their implications for the distribution of strain in incipient continental rifts. *Tectonics*, *39*. https://doi.org/10.1029/2019TC005834

Wedmore, L. N. J., Williams, J. N., Biggs, J., Fagereng, Å., Mphepo, F., Dulanya, Z., et al. (2020). Structural inheritance and border fault reactivation during active early-stage rifting along the Thyolo fault, Malawi. *Journal of Structural Geology*, *139*, 104097. https://doi.org/10.1016/j.jsg.2020.104097

Williams, J. N., Fagereng, Å., Wedmore, L. N. J., Biggs, J., Mphepo, F., Dulanya, Z., et al. (2019). How do variably striking faults reactivate during rifting? Insights from Southern Malawi. *Geochemistry, Geophysics, Geosystems*, *20*, 3588–3607. https://doi.org/10.1029/2019gc008219

Williams, J. N., Mdala, H., Fagereng, Å., Wedmore, L. N. J., Biggs, J., Dulanya, Z., et al. (2021). A systems-based approach to parameterise seismic hazard in regions with little historical or instrumental seismicity: Active fault and seismogenic source databases for southern Malawi. *Solid Earth*, *12*, 187–217. https://doi.org/10.5194/se-12-187-2021

Wölbern, I., Rümpker, G., Schumann, A., & Muwanga, A. (2010). Crustal thinning beneath the Rwenzori region, Albertine Rift, Uganda, from receiver-function analysis. *International Journal of Earth Sciences*, *99*, 1545–1557. https://doi.org/10.1007/s00531-009-0509-2

Yang, Z., & Chen, W.-P. (2008). Mozambique earthquake sequence of 2006: High-angle normal faulting in southern Africa. *Journal of Geophysical Research*, *113*. https://doi.org/10.1029/2007jb005419

Yu, Y., Liu, K. H., Reed, C. A., Moidaki, M., Mickus, K., Atekwana, E. A., & Gao, S. S. (2015). A joint receiver function and gravity study of crustal structure beneath the incipient Okavango Rift, Botswana. *Geophysical Research Letters*, *42*, 8398–8405. https://doi.org/10.1002/2015GL065811

Zhang, J., Bock, Y., Johnson, H., Fang, P., Williams, S., Genrich, J., et al. (1997). Southern California permanent GPS geodetic array: Error analysis of daily position estimates and site velocities. *Journal of Geophysical Research*, *102*, 18035–18055. https://doi.org/10.1029/97JB01380

References From the Supporting Information

Hammond, J. O. S., Kendall, J. M., Stuart, G. W., Keir, D., Ebinger, C., Ayele, A., & Belachew, M. (2011). The nature of the crust beneath the afar triple junction: Evidence from receiver functions. *Geochemistry, Geophysics, Geosystems*, *12*. https://doi.org/10.1029/2011GC003738

Hodgson, I., Illsley-Kemp, F., Gallacher, R. J., Keir, D., Ebinger, C. J., & Mtelela, K. (2017). Crustal structure at a young continental rift: A receiver function study from the Tanganyika Rift. *Tectonics*, *36*, 2806–2822. https://doi.org/10.1002/2017TC004477

Plasman, M., Tiberi, C., Ebinger, C., Gautier, S., Albaric, J., Peyrat, S., et al. (2017). Lithospheric low-velocity zones associated with a magmatic segment of the Tanzanian Rift, East Africa. *Geophysical Journal International*, *210*, 465–481. https://doi.org/10.1093/gji/ggx177